Defects in Zintl Compounds

DOI: 10.1002/anie.201311125

Defect-Controlled Electronic Properties in AZn_2Sb_2 Zintl Phases**

*Gregory S. Pomrehn, Alex Zevalkink, Wolfgang G. Zeier, Axel van de Walle, and G. Jeffrey Snyder**

Abstract: *Experimentally, AZn_2Sb_2 samples (A = Ca, Sr, Eu, Yb) are found to have large charge carrier concentrations that increase with increasing electronegativity of A. Using density functional theory (DFT) calculations, we show that this trend can be explained by stable cation vacancies and the corresponding finite phase width in $A_{1-x}Zn_2Sb_2$ compounds.*

Zintl compounds have enjoyed a rich history of scientific study since their initial investigation by Edward Zintl in the 1930s[1–3] and have recently gained interest for use in thermoelectric devices for power generation.[4,5] An opportunity now exists to combine the historical depth of chemical understanding, current experimental studies, and new computational capabilities to establish a detailed, coherent understanding of the electronic properties of Zintl materials. The concepts developed for Zintl phases are widely applicable in solid-state chemistry and can be used to understand the properties of many solid-state materials, from insulators and metals to semiconductors.

Within the Zintl–Klemm–Busmann concept,[3] the donation of valence electrons from the cation to the polyanionic sub-lattice is assumed to be complete. This simple concept is useful in understanding bonding and transport phenomena to first order, and can be employed quantitatively in doping Zintl compounds with alio-valent species.[6–8] In practice however, the degree of ionic bonding depends on the difference in electronegativity between the Zintl cation and the polyanion, and therefore on the covalent contributions to the bond. The degree of electron transfer between cations and anions[9] has well documented influence on the transport properties of Zintl compounds.[10,11] Consistent with the Zintl–Klemm–Busmann electron counting concept, density functional theory (DFT) studies show that, regardless of the covalent or ionic character of the cation bond, Zintl compounds have completely filled valence bands.[7,15–19] This suggests that Zintl phases, provided that the valence and conduction bands do not overlap, should exhibit intrinsic semiconducting behavior with a low concentration of charge carriers.[20]

Some Zintl phases exhibit large experimental p-type carrier concentrations that appear to challenge the definition of Zintl phases as valence-precise semiconductors. The AZn_2Sb_2 compounds (A = Ca, Sr, Eu, Yb) are an extreme example of such incongruity. AZn_2Sb_2 compounds form the $CaAl_2Si_2$ structure type (Figure 1 a, space group $P\bar{3}m1$), which is described by Burdett and Miller using the Zintl concept.[12]

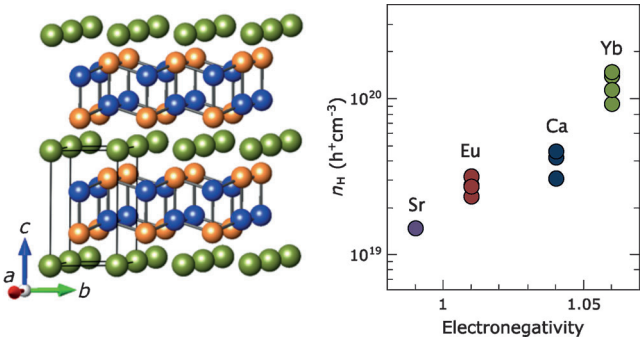

Figure 1. Left: Layered crystal structure of $SrZn_2Sb_2$, space group $P\bar{3}m1$. Sr, green; Zn, blue; Sb, orange. Right: The experimental Hall carrier concentration of AZn_2Sb_2 compounds increased with increasing cation electronegativity (Allred–Rochow scale[21,22]). The carrier concentration data were taken from Ref. [23–27].

The study of AZn_2Sb_2 phases has accelerated recently due to their excellent thermoelectric performance.[5,25–34] Good thermoelectric materials are generally extrinsically-doped semiconductors, with optimal carrier concentrations, n, on the order of 10^{19} to 10^{20} carriers/cm^3.[6,7,35,36] AZn_2Sb_2 (A = Ca, Sr, Eu, Yb) compounds possess large, nearly optimal carrier concentrations (ranging from 10^{19}–10^{20} holes/cm^3) without the need for doping—a unique feature among Zintl thermoelectrics. Remarkably, the experimentally observed carrier concentrations in AZn_2Sb_2 compounds trend with the electronegativity of A, as shown in Figure 1 b. Note that although the Allred–Rochow and Nagle electronegativity scales are consistent, other scales yield an overly high electronegativity for Eu.[37] The Sanderson electronegativity may be the most appropriate, but it has not been tabulated for rare earth elements.[38] The trend illustrated in Figure 1 is consistent across several research groups and synthetic approaches. The dependence of n on the cation electronegativity in AM_2Sb_2 compounds (M = Zn, Cd, Mn) has been exploited in several instances to optimize the thermoelectric figure of merit.[25,29,32]

The relationship between n and the electronegativity of A has been previously justified by imperfect electron donation from the cation, leading to electron-deficient polyanions, and

[*] G. S. Pomrehn, A. Zevalkink, W. G. Zeier, G. J. Snyder
Materials Science, California Institute of Technology
1200 East California Blvd, Pasadena, CA 91125 (USA)
E-mail: jsnyder@caltech.edu
Homepage: http://thermoelectrics.caltech.edu
A. van de Walle
School of Engineering, Brown University
Providence, RI 02912 (USA)

[**] A = Ca, Sr, Eu, Yb.

Supporting information for this article (computational details) is available on the WWW under http://dx.doi.org/10.1002/anie.201311125.

thus to holes in the valence band.[10,25] This is inconsistent with published computational results that confirm that the valence band is fully filled in each case. Here, we strengthen the Zintl concept with a consistent picture of valence-precise charge counting, electronic structure, and carrier concentration. Using DFT calculations, we show that the predicted concentration of *A*-site vacancies in AZn_2Sb_2 compounds depend strongly on the electronegativity of *A* and can explain the trend in the experimentally observed carrier concentrations.

The calculated electronic band structures for pure AZn_2Sb_2 compounds (A = Ca, Sr, Eu, Yb) are shown in Figure 2. All compounds are predicted to be semiconductors with the Fermi level falling within a forbidden gap region. While the variation in the calculated band gaps is within the

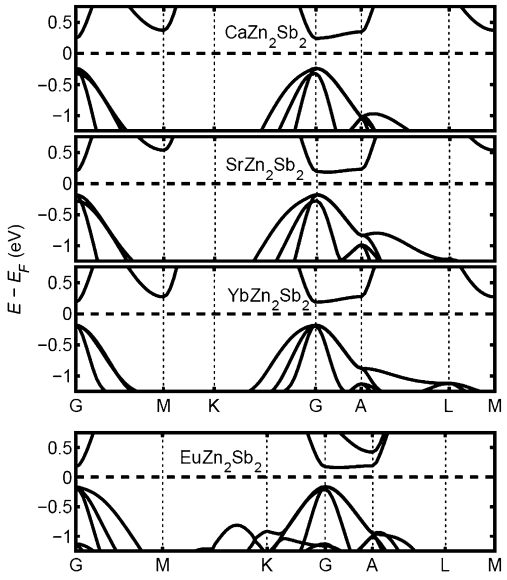

Figure 2. The electronic band structures of AZn_2Sb_2 compounds. The Fermi level at 0 K falls in the forbidden gap for each compound. An anti-ferromagenitic supercell was used for $EuZn_2Sb_2$ resulting in a different Brillouin zone, but the directions in reciprocal space are consistent.

range of experimental estimations (>0.25 eV[23]), the magnitude does not greatly influence the subsequent results. The structure of the valence band is also remarkably similar across the AZn_2Sb_2 series, each consisting of three bands with slightly different effective masses, consistent with previous studies indicating that the cation does not strongly influence states near the Fermi level.[13,14] In the case of A = Yb and Eu, the calculations suggest that the f-states are well below the valence band maximum and do not contribute significantly to character of these bonded states.

At 0 K, the valence band states are fully occupied and the conduction band states are unoccupied. This is consistent with a simple molecular orbital model[12] with 16 electrons per unit cell (including 2 electrons from the cation) completely filling the 8 bonding states per unit cell. Thus, for a perfect AZn_2Sb_2 crystal, thermally activated holes and electrons should dominate transport.[39] In contrast, experimental transport measurements show highly degenerate p-type behavior with little indication of thermally activated carriers up to 700 K. This indicates that in the measured samples, the Fermi level is near or inside the valence band, rather than near the middle of the band gap.

Since electronic structure calculations for pure AZn_2Sb_2 are inconsistent with experimental results, we investigate another explanation—that the degenerate p-type behavior is a result of non-stoichiometric samples containing stable site defects. For example, in the molecular orbital model, a deficiency of either *A*-site cations or Zn corresponds to an oxidation process, leading to fewer electrons in the bonding and anti-bonding states. The study of the effect of vacancies on the electronic properties of materials such as oxides has a long history (e.g., Ni^{2+} vacancies in NiO lead to p-type behavior).[40] Among Zintl phases, the influence of defects on transport has not yet been widely studied.

AZn_2Sb_2 phases are likely thermodynamically stable over a small, temperature-dependent composition range, the limits of which are determined by the energetics of configurational disorder and the equilibrium relationships with other nearby phases.[41,42] Unless a sample is cooled extremely slowly during synthesis, the phase at room temperature may also exist outside of its thermodynamic range of stability, due to kinetic limitations. A small deviation from the valence-precise stoichiometry can significantly alter the electronic properties.[43] For example, a vacancy concentration of only ≈ 0.6 at% of Yb atoms in $YbZn_2Sb_2$ could explain the large experimental p-type carrier concentration of $10^{20}\,h^+cm^{-3}$, assuming that each vacancy leads to two free carriers. Note that this latter assumption is challenged by the results below.

The site defect formation in AZn_2Sb_2 depends on the phase relationships with the other compounds in the Zn–Sb–*A* ternary phase diagram, which place thermodynamic limits on the chemical potential of each species. Based on total energy DFT calculations, we find that AZn_2Sb_2 phases are indeed stable at zero temperature with respect to the elemental constituents as well as to reported surrounding binary compounds (e.g., $CaSb_2$, $Ca_{11}Sb_{10}$).

For a crystal phase that has a small concentration of defects, we can consider them in the dilute limit[18] under the assumption that the defects are non-interacting and the crystal band structure is largely unaffected.[44] In this limit, we can employ the following relationship to calculate the concentration of defects ($x_{D,q}$) relative to the concentration of possible defect sites (x_o) as a function of the single defect enthalpy ($\Delta H = E_D - E_0$), the Fermi level (E_F) and the chemical potential of each atomic species (μ):

$$x_{D,q} \approx x_0 \exp\left(-\frac{\Delta H_{D,q}}{k_B T}\right) = x_0 \exp\left(-\frac{E_{D,q} - E_0 + qE_F + \mu}{k_B T}\right) \quad (1)$$

The chemical potential range for each species is constrained thermodynamically by nearby stable phases. Experimentally, nominally stoichiometric AZn_2Sb_2 samples are consistently found to contain ZnSb precipitates,[23–25,27] suggesting that some loss of *A* may occur during synthesis. Irrespective of how samples become *A*-deficient, the presence of ZnSb in all samples indicates that the two-phase equilibrium condition between AZn_2Sb_2 and ZnSb must be used to

explain the experimental trends. Thus, chemical potentials, μ, were chosen to match this condition. Requiring stability with the surrounding phases also limits the total defect concentration that can occur.

The total defect energy [E_D in Equation (1)] in each AZn_2Sb_2 phase was calculated after removing or replacing a single atom from a large supercell. Defect energies were calculated for vacancies on the A, Zn and Sb site (denoted V_A, V_{Zn}, and V_{Sb}, respectively), substitutions of Zn or Sb on the A site (Zn_A, Sb_A) or of A on the Zn site (A_{Zn}), and cation interstitials (A_i). The defect formation enthalpy, $\Delta H = E_D - E_0 + q E_F + \mu$, is often reported as a function of E_F, for a set of charged states, q.[45] Figure 3 (top) shows ΔH_D as

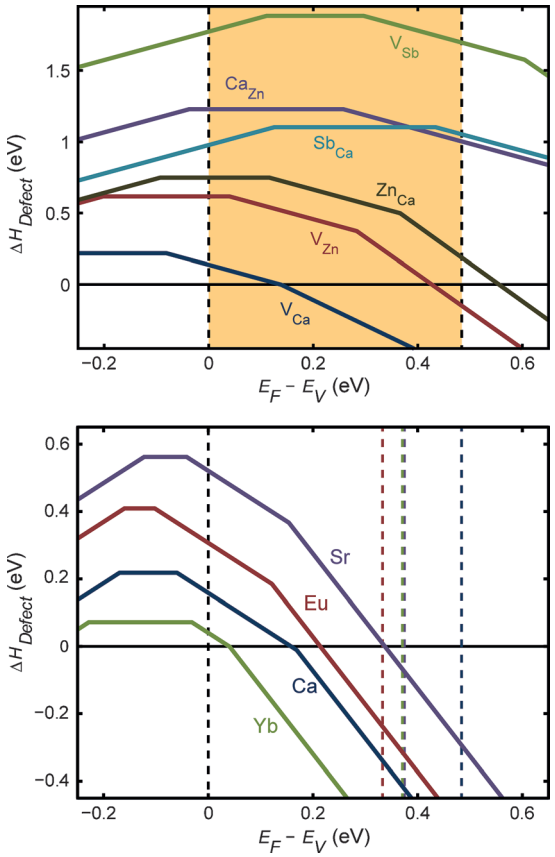

Figure 3. Top: The defect formation enthalpy, ΔH_{Defect} ($=\Delta H_D$) for various point defects in $CaZn_2Sb_2$ is shown as a function of E_F. In all AZn_2Sb_2 compounds, cation vacancies, V_A, were found to be the lowest energy defect. Bottom: With increasing cation electronegativity ΔH_D for cation vacancies decreases. The colored dashed lines correspond to the respective conduction band minima.

a function of E_F for all of the calculated defects in $CaZn_2Sb_2$. The slope of each line segment ($+1, 0, -1$ or -2) corresponds to the charged state of the defect. It is apparent from Figure 3 that vacancies on the Ca site (V_{Ca}) are the most energetically favorable point defect. This was found to be true for all AZn_2Sb_2 compounds—the A site cation vacancy always exhibits the lowest energy among the point defects considered. For this reason, we focus our attention on the cation vacancy defect energies across the AZn_2Sb_2 series.

Assuming equilibrium with ZnSb, the relevant reaction for the formation of a cation defect is given by Equation (2).

$$(1-x)\,AZn_2Sb_2 + (2\,x)\,ZnSb \rightarrow A_{1-x}Zn_2Sb_2 + x\,\Delta H_D \qquad (2)$$

The bottom panel of Figure 3 compares ΔH_D for A vacancies in each AZn_2Sb_2 phase (A = Ca, Sr, Eu, Yb). We find that $YbZn_2Sb_2$, the compound with the highest experimental hole concentration, has the smallest energy barrier for cation vacancy formation. A negative value of ΔH_D indicates that vacancies will form spontaneously. In general, vacancy formation is more energetically costly when the bonding is strong. The relationship between ΔH_D and electronegativity might be explained by the relative energy cost of transferring electrons from the cation to the anions, which in turn influences bond strength and vacancy formation energies. It may be impossible to construct an exact analytical model for ΔH_D based on electronegativity because of the complex interactions involved. Nevertheless, since DFT calculations include all interactions, we can exploit them to directly probe the influence of the cation bonding character in determining ΔH_D, and perhaps learn something about the influence of electronegativity on defects in the process.

The concentration of free charge carriers in AZn_2Sb_2 compounds is intimately tied to the thermodynamics of defect formation. The formation of negatively charged vacancies will shift the Fermi level downwards to maintain charge balance of free charge carriers (n_h and n_e), and charged defects ($x_{D,q}$) according to:

$$n_h - n_e + \sum_{D,q} q x_{D,q} = 0 \qquad (3)$$

The concentration of free holes and electrons, n_h and n_e, are also functions of E_F and the density of states, $g(E)$ through the following Fermi integrations:[39]

$$n_h = \int_{-\infty}^{E_V} g(E)[1 - f(E; E_F, T)]dE \qquad (4)$$

$$n_e = \int_{E_C}^{\infty} g(E) f(E; E_F, T) dE \qquad (5)$$

From Figure 3, it is clear that decreasing the Fermi level increases the formation enthalpy of the charged cation vacancies, thus reducing the concentration of vacancy defects. Thus, a delicate balance is struck between the equilibrium Fermi level and the concentration of defects and charge carriers. Contrary to expectations, each cation vacancy is found to lead to *fewer* than two free carriers on average, due to the different possible charge states ($0, -1, -2$) near $E_F = 0$.

An important consequence of these results is that n-type behavior in AZn_2Sb_2 compounds is thermodynamically unattainable. The low cation vacancy formation enthalpies effectively pin the Fermi level close to the valence band maximum. Any attempt to increase the Fermi level through n-type chemical doping would only encourage the formation of additional cation vacancies, preventing an increase of the Fermi level. This explains the persistent p-type character found in AZn_2Sb_2 compounds. The most dramatic case is

$YbZn_2Sb_2$, in which the Fermi level is pinned just above the valence band maximum. As temperature increases, the barrier to vacancy formation is more easily overcome and a higher vacancy concentration becomes stable—further shifting the Fermi level into the valence band.

The pseudo-binary phase diagram in Figure 4 illustrates the allowed concentration of cation vacancies in AZn_2Sb_2 as a function of temperature. The composition at the edge of each shaded region corresponds to the maximum concentration of vacancies at a given temperature, assuming equilibrium with ZnSb and free charge carriers. Any composition or temperature outside of the respective shaded regions results in the formation of $A_{1-x}Zn_2Sb_2$ at the highest allowed vacancy concentration (highest x) along with ZnSb precipitates.

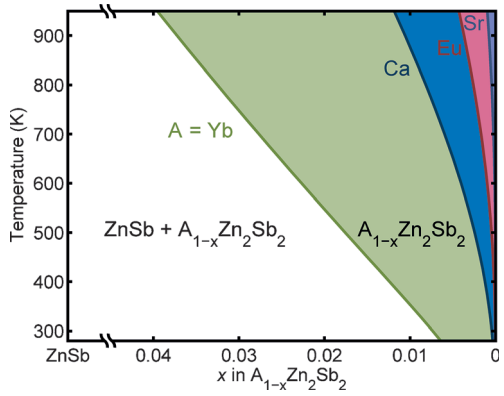

Figure 4. The pseudo-binary phase diagram shows the range of phase widths predicted for $A_{1-x}Zn_2Sb_2$. The boundary line for each phase corresponds to the maximum vacancy concentration for $A_{1-x}Zn_2Sb_2$ compounds in thermodynamic equilibrium with ZnSb.

Frequently, upon cooling a sample below a certain material-dependent temperature, diffusion kinetics become too slow to fully equilibrate the system. Below this threshold temperature, the concentration of ZnSb precipitates and the vacancy concentration in AZn_2Sb_2 may become effectively "frozen". The vacancy concentration and corresponding carrier concentration thus becomes temperature-independent below the threshold temperature, giving rise to the temperature-independent carrier concentration observed experimentally. If high enough vacancy concentrations (e.g. greater than 3 at% in $YbZn_2Sb_2$) are maintained at room temperature, these may be detectable experimentally by high quality X-ray diffraction, warranting further investigation.

The estimated defect and hole carrier concentrations for AZn_2Sb_2 compounds are listed in Table 1, assuming that the defect concentration becomes kinetically limited ("frozen") at 800 K. Our results show striking qualitative and quantitative agreement with the experimental Hall carrier concentrations reported in these compounds ($n_{h,exp}$ in Table 1). These results suggest that the experimental trend shown in Figure 1 between the cation electronegativity and n in AZn_2Sb_2 compounds relates to the intrinsically formed cation vacancies. This mechanism may be generally applicable, perhaps

Table 1: The calculated cation vacancy concentrations, $[V_A]$, carrier concentrations, n, and predicted Hall carrier concentrations, n_H, at 800 K are consistent with experimental Hall carrier concentrations, $n_{H,exp}$, at room temperature. All concentrations are reported as $10^{19}\,cm^{-3}$.

	$[V_A]$ (800 K)	n (800 K)	n_H (800 K)	$n_{H,exp}$ (300 K)
$SrZn_2Sb_2$	0.36	0.52	1.0	1.5
$EuZn_2Sb_2$	2.0	2.5	2.9	2.5
$CaZn_2Sb_2$	6.3	6.0	6.2	4.0
$YbZn_2Sb_2$	22	16	16	12

explaining similar trends seen in $A_{14}MnSb_{11}$, and $A_9Zn_{4.5-x}Sb_9$ (A = Yb or Ca) based materials.[10,11]

AZn_2Sb_2 samples (A = Ca, Sr, Eu, Yb) are consistently found to have large carrier concentrations that increase with increasing electronegativity of the A cation, despite DFT results placing the Fermi level in the middle of the band gap in each case. Here, we have demonstrated that large concentrations of thermodynamically stable cation vacancies are possible in AZn_2Sb_2 phases, and can explain the trend in experimental carrier concentrations.

Electronegativity influences the degree of electron transfer between the anion and cation in a bond, but it does not *directly* affect the total number of electrons in the valence band or the concentration of free carriers (assuming the valence state of the cation is unaltered). However, the bonding character does appear to influence the bond strength and lattice energy, and, in turn, affect the thermodynamically stable concentration of lattice defects. In this way, the electronegativity of the cation may *indirectly* affect the electronic carrier concentration.

Our computational results confirm that the defect energies of A-site cation vacancies follow the same trend observed experimentally. These results suggest that cation vacancies are the primary mechanism responsible for varying the carrier concentration in nominally valence-precise AZn_2Sb_2 compounds. These results may shed light on similar trends seen in other Zintl systems, leading to new strategies for designing functional, complex semiconductors.

Received: December 21, 2013
Published online: February 24, 2014

Keywords: defect formation · electronic transport · phase stability · Zintl phases

[1] H. Schaefer, *Annu. Rev. Mater. Sci.* **1985**, *15*, 1–41.
[2] S. M. Kauzlarich, *Chemistry, Structure, and Bonding of Zintl Phases and Ions*, Wiley-VCH, Weinheim, **1996**.
[3] H. Schäfer, B. Eisenmann, W. Mueller, *Angew. Chem.* **1973**, *85*, 742–760; *Angew. Chem. Int. Ed. Engl.* **1973**, *12*, 694–712.
[4] E. S. Toberer, A. F. May, G. J. Snyder, *Chem. Mater.* **2010**, *22*, 624–634.
[5] G. J. Snyder, E. S. Toberer, *Nat. Mater.* **2008**, *7*, 105–114.
[6] E. S. Toberer, C. A. Cox, S. R. Brown, T. Ikeda, A. F. May, S. M. Kauzlarich, G. J. Snyder, *Adv. Funct. Mater.* **2008**, *18*, 2795–2800.
[7] A. Zevalkink, W. G. Zeier, G. Pomrehn, E. Schechtel, W. Tremel, G. J. Snyder, *Energy Environ. Sci.* **2012**, *5*, 9121.

[8] E. S. Toberer, A. Zevalkink, N. Crisosto, G. J. Snyder, *Adv. Funct. Mater.* **2010**, *20*, 4375 – 4380.
[9] R. T. Sanderson, *Science* **1951**, *114*, 670.
[10] C. A. Uvarov, F. Ortega-Alvarez, S. M. Kauzlarich, *Inorg. Chem.* **2012**, *51*, 7617 – 7624.
[11] S. Bobev, J. D. Thompson, J. L. Sarrao, M. M. Olmstead, H. k. Hope, S. M. Kauzlarich, *Inorg. Chem.* **2004**, *43*, 5044 – 5052.
[12] J. K. Burdett, G. J. Miller, *Chem. Mater.* **1990**, *2*, 12 – 26.
[13] P. Alemany, M. Llunell, E. Canadell, *J. Comput. Chem.* **2008**, *29*, 2144 – 2153.
[14] C. Kranenberg, D. Johrendt, A. Mewis, *Z. Anorg. Allg. Chem.* **1999**, *625*, 1787 – 1793.
[15] H. He, R. Stearrett, E. R. Nowak, S. Bobev, *Inorg. Chem.* **2010**, *49*, 7935 – 7940.
[16] S.-J. Kim, M. G. Kanatzidis, *Inorg. Chem.* **2001**, *40*, 3781 – 3785.
[17] G. S. Pomrehn, E. S. Toberer, G. J. Snyder, A. van de Walle, *J. Am. Chem. Soc.* **2011**, *133*, 11255 – 11261.
[18] G. S. Pomrehn, E. S. Toberer, G. J. Snyder, A. van de Walle, *Phys. Rev. B* **2011**, *83*, 094106.
[19] P. H. M. Böttger, G. S. Pomrehn, G. J. Snyder, T. G. Finstad, *Phys. Status Solidi A* **2011**, *208*, 2753 – 2759.
[20] R. Nesper, *Prog. Solid State Chem.* **1990**, *20*, 1 – 45.
[21] A. L. Allred, E. G. Rochow, *J. Inorg. Nucl. Chem.* **1958**, *5*, 264 – 268.
[22] E. J. Little, Jr., M. M. Jones, *J. Chem. Educ.* **1960**, *37*, 231 – 233.
[23] E. S. Toberer, A. F. May, B. C. Melot, E. Flage-Larsen, G. J. Snyder, *Dalton Trans.* **2010**, *39*, 1046 – 1054.
[24] A. F. May, M. A. McGuire, J. Ma, O. Delaire, A. Huq, R. Custelcean, *J. Appl. Phys.* **2012**, *111*, 033708.
[25] F. Gascoin, S. Ottensmann, D. Stark, M. S. Haile, G. Snyder, *Adv. Funct. Mater.* **2005**, *15*, 1860 – 1864.
[26] H. Zhang, J. T. Zhao, Y. Grin, X. J. Wang, M. B. Tang, Z. Y. Man, H. H. Chen, X. X. Yang, *J. Chem. Phys.* **2008**, *129*, 164713.
[27] C. Yu, T. J. Zhu, S. N. Zhang, X. B. Zhao, J. He, Z. Su, T. M. Tritt, *J. Appl. Phys.* **2008**, *104*, 013705.
[28] K. Guo, Q.-G. Cao, X.-J. Feng, M.-B. Tang, H.-H. Chen, X. Guo, L. Chen, Y. Grin, J.-T. Zhao, *Eur. J. Inorg. Chem.* **2011**, 4043 – 4048.
[29] H. Zhang, L. Fang, M. B. Tang, Z. Y. Man, H. H. Chen, X. X. Yang, M. Baitinger, Y. Grin, J. T. Zhao, *J. Chem. Phys.* **2010**, *133*, 194701.
[30] H. Zhang, L. Fang, M.-B. Tang, H.-H. Chen, X.-X. Yang, X. Guo, J.-T. Zhao, Y. Grin, *Intermetallics* **2010**, *18*, 193 – 198.
[31] H. Zhang, M. Baitinger, M. B. Tang, Z. Y. Man, H. H. Chen, X. X. Yang, Y. Liu, L. Chen, Y. Grin, J. T. Zhao, *Dalton Trans.* **2010**, *39*, 1101 – 1104.
[32] Q.-G. Cao, H. Zhang, M.-B. Tang, H.-H. Chen, X.-X. Yang, Y. Grin, J.-T. Zhao, *J. Appl. Phys.* **2010**, *107*, 053714.
[33] X.-J. Wang, M.-B. Tang, H.-H. Chen, X.-X. Yang, J.-T. Zhao, U. Burkhardt, Y. Grin, *Appl. Phys. Lett.* **2009**, *94*, 092106.
[34] Ref. [28].
[35] A. Zevalkink, G. S. Pomrehn, S. Johnson, J. Swallow, Z. M. Gibbs, G. J. Snyder, *Chem. Mater.* **2012**, *24*, 2091 – 2098.
[36] A. Zevalkink, E. S. Toberer, W. Zeier, E. Flage-Larsen, G. J. Snyder, *Energy Environ. Sci.* **2011**, *4*, 510 – 518.
[37] J. K. Nagle, *J. Am. Chem. Soc.* **1990**, *112*, 4741.
[38] A. Ormeci, A. Simon, Y. Grin, *Angew. Chem.* **2010**, *122*, 9182 – 9186; *Angew. Chem. Int. Ed.* **2010**, *49*, 8997 – 9001.
[39] C. Kittel, *Introduction to Solid State Physics*, Wiley, Hoboken, **2004**.
[40] P. A. Cox, *Electronic Structure and Chemistry of Solids*, Oxford Science, Oxford, **1987**.
[41] J. W. Gibbs, *On the Equilibrium of Heterogeneous Substances.*
[42] J. F. Shackelford, *Introduction to Materials Science for Engineers*, Prentice Hall, Englewood, **2009**.
[43] L. Bjerg, G. K. H. Madsen, B. B. Iversen, *Chem. Mater.* **2012**, *24*, 2111 – 2116.
[44] Y. Takagiwa, Y. Pei, G. S. Pomrehn, G. Snyder, *Appl. Phys. Lett.* **2013**, *1*, 011101.
[45] A. Zunger, *Appl. Phys. Lett.* **2003**, *83*, 57.

